Phase Behavior and Morphology of Poly(ethylene oxide) Blends

S. Balijepalli and J. M. Schultz*

Department of Chemical Engineering, University of Delaware, Newark, Delaware 19716

J. S. Lin

Oak Ridge National Laboratory,† Oak Ridge, Tennessee 37831-6393

Received May 7, 1996; Revised Manuscript Received June 25, 1996⊗

ABSTRACT: Crystallization studies on blends of high and low molecular weight poly(ethylene oxide) (PEO) have been carried out to characterize phase behavior and morphology. At low crystallization temperatures, both components cocrystallize into a common crystal lattice. The thickness of the cocrystal is found to vary with the blend composition. At high fractions of the low molecular weight polymer, the cocrystal is thin, suggesting a folding of the long-chain polymer into the lattice of the low molecular weight chain. At lower fractions of the low molecular weight polymer, the cocrystal is thicker, resembling the higher molecular weight polymer. At higher crystallization temperatures, the components form a defective cocrystal which dynamically phase splits into its components. The crystal transformation in the blend occurs by thinning of low molecular weight chains and thickening of high molecular weight chains. The formation of crystal templates of both components eventually results in phase-segregated growth. Models for cocrystallization and dynamic phase separation of components are discussed. A time-resolved small-angle X-ray scattering study along with complementary calorimetry and optical microscopy results confirms the mechanism of cocrystallization and dynamic phase separation in PEO blends.

1. Introduction

Poly(ethylene oxide) (PEO) has been one of the most extensively studied linear polymers. In the past three decades, melt crystallization studies of the polymer have been carried out for all molecular weight ranges. In particular, the work of Kovacs and co-workers[1−4] on crystallization from the melt of low molecular weight PEO fractions ($M_w = 2000-10000$) is extremely interesting. It was shown that small chains crystallize with molecules either fully extended or folded an integral multiple, n, of times (1−3). The thickness of the crystal increases stepwise as a function of the undercooling, with the fully extended crystals formed at the highest crystallization temperatures, very close to the melting point of the polymer. At lower temperatures, there is a stepwise decrease in the crystal thickness, corresponding always to an integer folding of chains. Isothermal growth rates also decrease with undercooling, in a stepwise fashion, with the breaks in the growth rate of single crystals corresponding to the transition in number of folds of the polymer chain. Growth and morphology data have been complemented with thickening and melting behavior of PEO crystals with increasing temperature and/or time. It has been shown that for short-chain PEO, the most stable or equilibrium crystal corresponds to the fully extended chain and that the higher folded chain crystals are a metastable state. The existence of an integer number of folds in short-chain PEO was explained by the need of the crystal to completely exclude from the crystal the chain ends, which have hydroxyl end groups. A possible network of hydrogen bonding at the surface may also lead to a decrease in the surface energy.

In subsequent work by Cheng and co-workers[5−7] on low molecular weight PEO fractions, it was shown that nonintegral folding (NIF) chain crystals form initially and then rapidly transform to integral folded (IF) crystals. The transformation occurs through a thickening and thinning of crystals. The NIF crystal corresponds to an inclusion of chain ends in the lattice, which makes it a defect structure formed because of the relatively fast kinetics of growth. The transformation to IF crystals would represent a thermodynamic driving force of increasing the stability of the crystal, with chain ends being fully excluded from the lattice. Equivalent work on short-chain PEO with modified end groups was done as early as the mid 1970s by Booth and co-workers[8−10] and more recently by Cheng and co-workers.[11,12] Time-resolved small-angle and wide-angle X-ray scattering, along with DSC measurements, have led to the conclusion that thickening or thinning of the NIF crystals is slow for chains with large end groups. This would be consistent with a slower diffusional translation of chains with bulky end groups through the crystal lattice.

As the molecular weight of the chain is increased, the integral number of folding of PEO chains into crystals gives way to a more continuous distribution of crystal sizes. The study of intermediate molecular weight fractions ($M_w = 10^4-10^6$) of polydispersity 1.2 and 2 was reported in the 1980s.[13,14] Morphology and crystal growth rate studies were reported. It was shown that PEO crystallized with different kinetic coefficients as a function of the undercooling. At lower undercooling, the coefficient corresponded to "Regime I" behavior, the crystal growth rate being controlled by the secondary nucleation of a chain on a crystal lattice.[15,16] At higher undercooling, there is a transition to "Regime II" behavior, the crystal growth rate being controlled by a lateral spreading rate of chains on the crystal surface. The morphology observed also changed from incomplete spherulites (called "hedrites") to spherulites in going from Regime I to Regime II. Subsequent work on intermediate fractions ($M_w = 23000-105000$)[17] has revealed three transition points, a Regime II/Regime I transition at $\Delta T = 8.5$ K, a Regime I/Regime II transition at $\Delta T = 10.5$ K, and a Regime II/Regime III transition at $\Delta T = 17.5$ K. Regime III corresponds to a crystal growth rate of a multilayered, multinucleation

* Author to whom all correspondence should be addressed.
† Managed by Martin-Marietta Energy Systems, Inc.
⊗ Abstract published in *Advance ACS Abstracts,* August 15, 1996.

S0024-9297(96)00678-X CCC: $12.00

Table 1. Molecular Weights, Polydispersities, and Suppliers

mol wt (M_w)	polydispersity (M_w/M_n)	supplier
270000	1.1	Pressure Chemical Co.
5000	1.05	Polysciences Inc.

mechanism.[18] The morphology also changed, as observed by polarized light microscopy.

A study of binary mixtures of PEO of high and low molecular weight was carried out by Cheng[19−21] to characterize the growth rates and phase behavior of the blends. Blends of molecular weight 3500−20000 with molecular weight 100000 were studied. At low undercoolings, the two components were found to cocrystallize and at higher undercoolings, to phase segregate. They concluded that molecular segregation in the mixtures occurs before the temperature reaches the equilibrium melting point of the low molecular weight fraction. The behavior was characterized by DSC and optical microscopy. Subsequent studies of mixtures using TEM[22,23] were carried out to determine the morphology of the blends. A suitable etching methodology was developed to examine the microstructures.

In this paper, we report the study of crystallization of PEO mixtures of molecular weight 5000 (5K) and 270000 (270K) as a function of composition and temperature of crystallization. A time-resolved, small-angle X-ray scattering (SAXS) study of the crystallization of the blends, along with complementary thermal analysis and optical microscopy, has been carried out. At low temperatures of crystallization, the two components are found to cocrystallize. Time-resolved SAXS of the blends at these temperatures shows that the size of the cocrystals that are formed varies with the composition of the blend. For a blend containing a high fraction of the low molecular weight, the cocrystals are thin, corresponding to the folding of the long-chain molecule of the high molecular weight polymer into the lattice of the smaller. At higher composition of the high molecular weight fraction, the cocrystals are thicker, resembling the crystals of the pure high molecular weight fraction. At higher crystallization temperatures, we report the dynamic phase separation of the two components. Time-resolved SAXS data for the blends show that the two components cocrystallize first to form a defect structure. The components in the cocrystal subsequently thin and thicken, leading to a dynamic phase splitting of the blend components. The thinning and thickening of small molecular weight chains in a pure fraction has been well studied. Here we report an analogous behavior in the blend. The long-chain crystals are found to thicken, a process which does not occur in the neat polymer, and the short-chain crystals thin down to exclude chain ends from the crystal lattice. The phase splitting is shown to lead to phase segregation. At higher crystallization temperatures, both components crystallize in phase-segregated areas. Complementary thermal analysis along with optical microscopy is reported to confirm the mechanism of phase segregation.

2. Experimental Section

2.1. Materials and Blends. PEO fractions along with their characterization data and supplier are listed in Table 1. The polydispersities of the samples were taken to be those provided by the vendor. Both components are narrow fractions. Blends of the PEO fractions were prepared by dissolving the two components in benzene and solution casting them in a nonsolvent of isooctane. The resulting powders were dried in a vacuum oven for a week, and the solvent content of the samples was checked by thermal gravimetric analysis (TGA). The compositions of blends prepared were 50/50 70/30 and 80/20, where the 70 and 80 correspond to the weight fraction of the low molecular weight polymer. Powders of the blend were melted to prepare appropriate samples for measurements.

2.2. Optical Microscopy. Optical microscopy (OM) studies were carried out with a Nikon Microphot-SA microscope in conjunction with a Mettler hot stage (FP-82). Powders of the sample weighing ∼5−7 mg were melted on glass slides with cover slips to form thin films ∼20−50 μm thick. The specimens were heated to 90 °C to melt the film and were then quickly inserted into a hot stage set at a pre-fixed crystallization temperature. The hot stage was calibrated with a melting point standard and the temperature control was ±0.2 K. The growth of spherulites was recorded on a VCR, and an image analysis program was used to extract growth rate data from time-lapsed frames of spherulitic fronts. Polarized light and Hoffman modulation contrast optics were utilized to observe the morphology. In addition, photographs were taken with a 35 mm camera.

2.3. Differential Scanning Calorimetry. Differential scanning calorimetry (DSC) was carried out with a Perkin-Elmer DSC7 system. Typical sample weights were 6−8 mg. The DSC was calibrated with an indium standard for temperature and heat flow. The temperature control was ±0.2 K. Samples were melted at a temperature of 90 °C and quenched to the isothermal crystallization temperature to record the exothermic crystallization processes. The samples were crystallized and then heated to above their melting temperature from the crystallization temperature to record the melting endotherm. A standard heating rate of 20 °C/min was used unless otherwise indicated. All melting temperatures reported refer to peak temperatures corrected for heating rate. Temperatures were not corrected for thermal lag.

2.4. Small-Angle X-ray Scattering. Time-resolved small-angle X-ray scattering (SAXS) was performed on the ORNL 10-m SAXS instrument,[24,25] with a sample−detector distance of 5.06 m, using Cu Kα radiation (λ = 1.54 Å) and a 20 × 20 cm^2 position-sensitive area detector with a cell (element) of about 3 × 3 mm. The scattering intensity was stored in a 64 × 64 data array. Corrections were made for the instrumental background and detector efficiency (via an ^{55}Fe radioactive standard which emits γ-rays isotropically) on a cell-by-cell basis. The data were azimuthally averaged in the q range $0.022 < q < 1.058$ nm^{-1} ($q = (4\pi/\lambda)\sin(\theta/2)$, where λ is the X-ray wavelength and θ is the scattering angle) and converted to an absolute cross section by means of precalibrated secondary standards.[24] The absolute intensity is in C min^{-1}. Samples weighed ∼50 mg and were ∼1.5 mm thick. The samples were melted on a hot stage and inserted into a cell placed in the path of the X-rays, maintained at the isothermal crystallization temperature. The chamber was evacuated before X-ray scattering data were collected. Time-resolved synchrotron small-angle X-ray scattering of the 50/50 blend was also carried out at the X3A2 beam line at the National Synchrotron Light Source (NSLS). The X-ray beam was focused by a Si crystal monochromator with a beam size of 0.1 × 0.1 mm. The wavelength of X-rays was λ = 1.54 Å. A Braun OED 50 mm position-sensitive detector was used to collect X-ray scattering data. A temperature-jump hot stage was used to carry out the isothermal experiments.[26] The scattering data were corrected for background. The background was taken to be the average scattering intensity of the initial melt files. No desmearing was performed, due to the high degree of collimation and its very small cross section. The melt-corrected files were smoothed by two procedures: (1) A median smoothing of scattering curve was done to eliminate any outlier points. This is particularly useful at large angles of scattering, whereby the smoothed curve passes through a cluster of points, leaving out stray data points. (2) The data were subsequently smoothed with a Butterworth low-pass filter, preserving peak shape and heights. The following parameters have been extracted from the data: (1) long period, i.e., the average distance of lamellar crystals separated by amorphous regions,

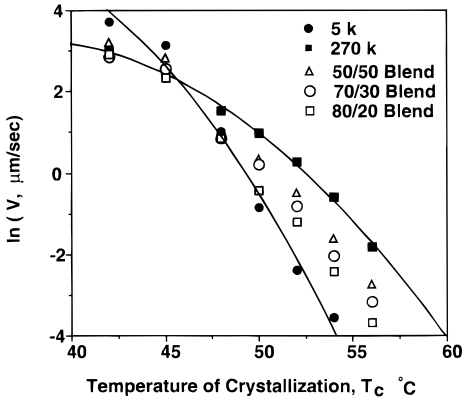

Figure 1. Spherulitic growth rates obtained from optical microscopy studies on pure fractions and blends. Note the crossover region at a crystallization temperature of 45 °C; the 5K polymer grows faster than the 270K polymer.

from the maximum of the Lorentz-corrected SAXS interference peaks; (2) the invariant (Q), i.e., the integral over reciprocal space of the intensity scattered in the scattering range.

3. Results

Figure 1 represents the growth rate of PEO pure fractions and blends obtained from optical microscopy. The standard deviation of the measurements are the lowest for slow growth to about 15% error for fast growth rates. The principal error in measurements at fast growth rate is due to the error in the capture of time-lapsed frames. The low molecular weight polymer grows slowly compared to the high molecular weight, due to the smaller driving force available to it. However, at low temperatures of crystallization, it is seen that there exists a crossover region where the low molecular weight fraction grows at a much higher rate. This crossover can be attributed to two reasons: (1) the kinetic coefficient of growth is higher for the low molecular weight and (2) at lower temperatures, diffusional limitations in the high molecular weight sample result in reduced growth rate. The growth rate of the blends lies intermediate to the pure fractions.

For the short range of crystallization temperatures (42−54 °C), the growth rates of pure fractions do not show any breaks. The data for the pure fractions are fitted to the nucleation theory as given by[15,16]

$$V = A_f \exp[-U^*/R(T_c - T_\infty)] \times \exp[-K_g/T_c(\Delta T)f] \quad (1)$$

where $f = 2T_c/(T_m^0 + T_c)$, $K_g = 4b\sigma\sigma_e T_m^0/k_b\Delta H_f$, T_c is the crystallization temperature and T_m^0 is the equilibrium melting temperature of the pure fraction polymer, T_∞ is a theoretical temperature at which all motion associated with viscous flow stops, σ is the lateral surface energy, σ_e is the fold surface energy in the crystal, b is the distance between lattice planes for the growth direction (b = 0.462 nm for 120 planes), k_b is the Boltzmann constant, A_f is the preexponential factor, and U^* is the activation energy of transport of polymer chains across the melt/crystal interface. The equilibrium melting temperatures are deduced from DSC analysis and are 63.2 and 70.2 °C for the 5K and 270K pure fractions, respectively. The value of T_∞ was taken to be by definition T_g − 30 K with T_g of PEO at −67 °C. The quantity U^* is a value 29.3 kJ/mol taken from the work of Kovacs.[3] The factor 4 in K_g has been chosen to be consistent with Regime III of crystallization observed

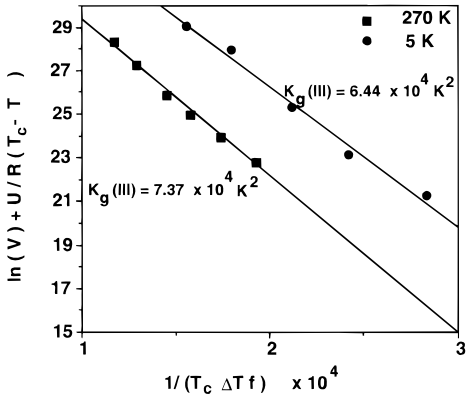

Figure 2. Plot of ln (V) + $U^*/R(T_c - T)$ vs $1/(T_c\Delta Tf)$ for the pure fractions. Regime III theory of secondary nucleation[18] was utilized to fit the growth data. Slopes of the fit, give the kinetic coefficient $K_g(III) = 4b\sigma\sigma_e T_m^0/k_b\Delta H_f$.

Table 2. Average $\sigma\sigma_e$ Determined from Spherulitic Growth Rates: Comparison of Values Obtained in This Work and Previous Work

M_w	regime	$\sigma\sigma_e$ (erg^2 cm^{-4})
	Work of Kovacs[3]	
2000	II	393
4000	II	416
6000	II	423
10000	II	407
	Work of Cheng and Co-workers[17]	
23000	III	264
56300	III	273
105000	III	274
	This Work	
5000	III	345
270000	III	390

in the pure polymers. For the high molecular weight fraction (270K), the undercooling is from 16 to 28 K. The observed Regime II/Regime III transition occurs at about ΔT of 17 K in polymers of $M_w \sim 100000$.[3,17] For the low molecular weight fraction (5K), comparing with Kovacs[3] data on PEO of molecular weights 4000 and 6000, it is seen that only a single growth rate exists without a break at the undercoolings of interest in this work. We will assume that the same mechanism of Regime III is operative. Figure 2 is a fit of (1) to the data for the pure fractions. The values of $\sigma\sigma_e$ calculated are tabulated in Table 2, along with the estimation of Kovacs[2] and Cheng.[17] It is interesting to note that the fold surface energy of the low molecular weight is lower than that of the high molecular weight, presumably because most of the undercooling goes to bending the chains. Thus at $T_c \sim 40$ °C and lower, in spite of the lower driving force present for the 5K chains, the growth rate is higher than the 270K material, due to the smaller concentration of folds in twice-, once-, or non-folded-chain crystals, relative to the fully chain-folded crystals associated with the higher molecular weight. This has relevance for crystallization in blends, where at these temperatures cocrystals of the blend are formed. The faster growing component provides the templates on which the other component can add. In our case, the 270K chain adds onto the template of the 5K crystals, resulting in cocrystals that have the thickness of the pure 5K crystals.

The morphology observed is seen in Figure 3. The high molecular weight chain grows as a compact spherulite (Figure 3a). Blending results in open structures, as in Figure 3b. At higher temperatures of crystallization, the spherulites are open, indicating that segrega-

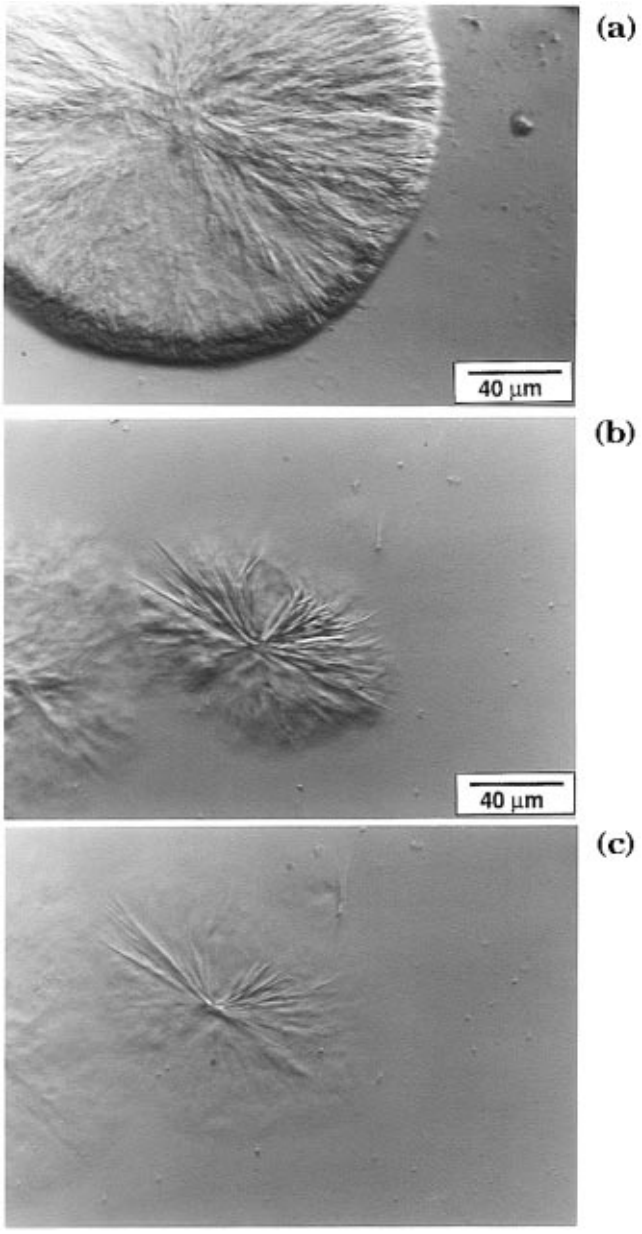

Figure 3. (a) Growth of a compact spherulite of 270K at T_c = 54 °C. (b) Growth of an open spherulite of the 80/20 blend at T_c = 54 °C. Segregation of 5K polymer results in two areas: an open structure of thick bundles and a diffuse region intermediate to regions of thick bundles. (c) Melting of the spherulite of the 80/20 blend. The diffuse regions melt away first, leaving behind the thicker bundles, indicative of two crystal populations of thick and thin crystals.

tion effects of the low molecular weight become important. At lower temperatures, the spherulites are compact. This is true of all blend compositions. At the same crystallization temperature, a 50/50 blend grows as a compact spherulite, as against relatively more open structures of the 70/30 and 80/20 blends. There exist two regions within the spherulite, one consisting of thicker bundles and the other a diffuse region filling between the thicker bundles. Melting of the spherulite results in the melting of the diffuse region first, followed by melting of the thicker bundles, indicating the presence of two crystal populations (Figure 3c).

Isothermal crystallization and melting behavior of the pure fractions and blends as studied by DSC characterizes the phase behavior of the blends. Results of crystallization half-times and of the nature of the exotherms

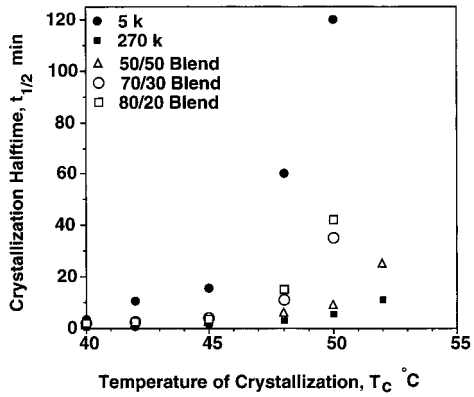

Figure 4. Half-times of isothermal crystallization for the pure fractions and blends obtained by DSC. Crystallization half-times for the blends are closer to the high molecular weight polymer 270K.

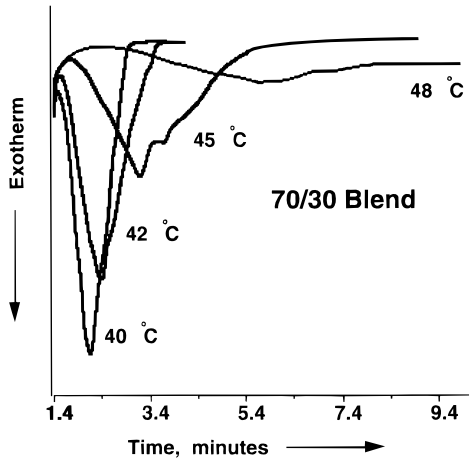

Figure 5. Crystallization exotherms obtained in the DSC for the 70/30 blend at isothermal crystallization temperatures of 40−48 °C. At 40 °C and lower, a single crystallization peak is obtained. At 45 °C and higher, a broad crystallization peak with a shoulder is obtained.

for the materials are described first, followed by the melting behavior of the samples.

The crystallization half-times of the materials studied are plotted as a function of the temperature of crystallization in Figure 4. At low T_c, the crystallization half-times of the high and low molecular weight fractions are comparable. The half-times at these temperatures indicate a rapid transformation rate of both the components. At higher T_c or lower undercooling, the crystallization half-time of the 5K fraction increases rapidly, diverging from the half-time of the 270K fraction. The half-times for the blends are intermediate to the two fractions but lie closer to the 270K fraction. The nature of the crystallization exotherms for the 70/30 blend for increasing T_c are shown in Figure 5. At the lowest temperature (40 °C), there is a single crystallization peak. At higher T_c, the crystallization exotherm broadens to include a shoulder (T_c = 45 °C and higher). A broad exotherm indicates that both components may have crystallized simultaneously instead of sequentially in the blend in spite of the 5K fraction having a slow rate of transformation compared to the 270K fraction. The crystallization exotherms for the 50/50 and 80/20 blends are similar to those of the 70/30 blend.

The melting behavior of the blends and pure fractions is shown in Figure 6a−c. A heating rate of 20 °C/min has been used, starting from the temperature of crystallization. Figure 6a shows the melting endotherm for

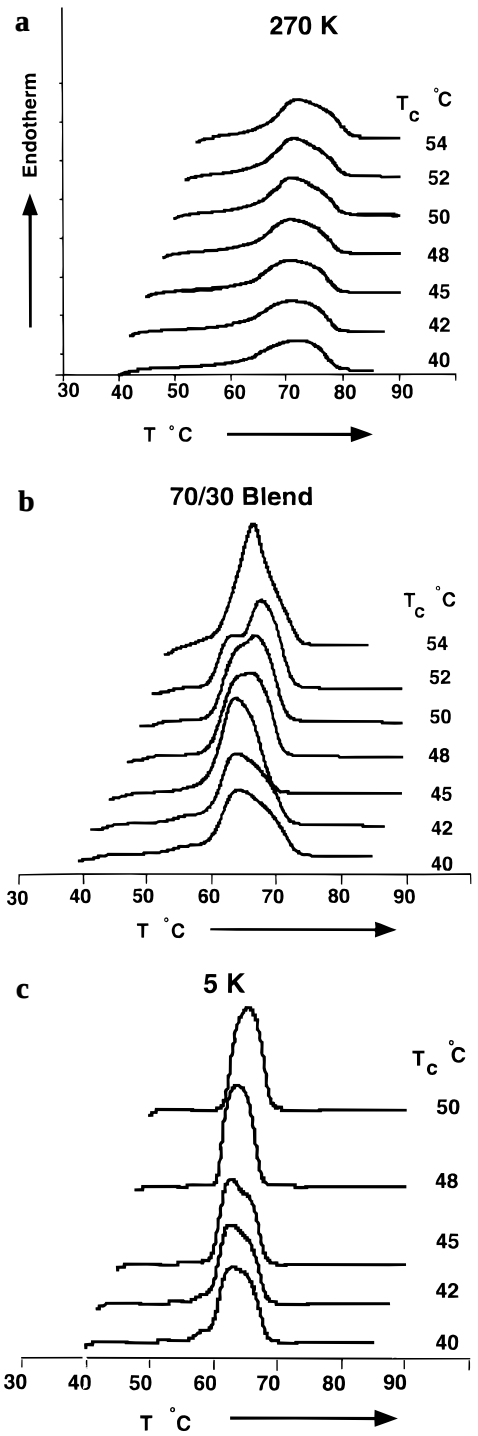

Figure 6. Melting endotherm of pure fractions and 70/30 blend obtained in the DSC. Samples were isothermally crystallized and melted from the crystallization temperature by ramping at 20 °C/min. (a) 270K, a single melting peak; (b) 70/30 blend, a double melting peak from 48 °C and higher; (c) 5K, melting peaks attributed to integral folded crystals.

the 270K fraction. The peak melting temperatures increase slowly with increasing T_c. Figure 6c shows similar results for the 5K chain. For the low molecular weight fraction as reported before,[3,4,19] we get multiple melting peaks. The multiple melting peaks are attributed to the existence of the short chain in the following configurations: fully extended (IF = 0), once folded (IF = 1), and twice folded (IF = 2). At low temperatures of crystallization (40 °C and lower), there are three distinct melting peaks. The small melting peak at ~58 °C corresponds to a thin IF = 2 crystal and

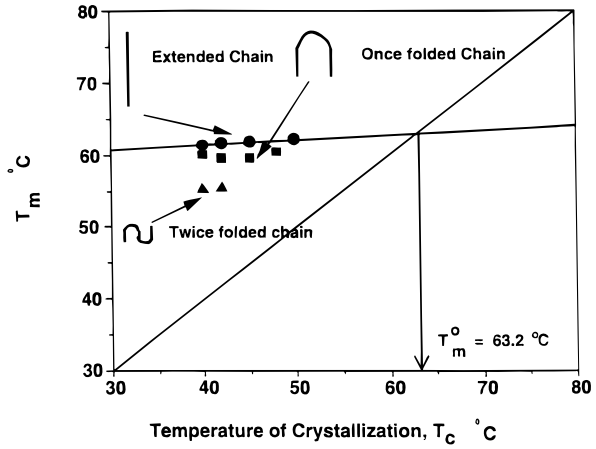

Figure 7. Hoffman−Weeks plot of T_m vs T_c. The equilibrium temperature of the 5K polymer is T^0_m = 63.2 °C.

the melting peak at ~62 °C to an IF = 1 crystal. The melting peak of the extended chain is superimposed on the melting of the IF = 1 crystal at these temperatures but becomes distinct at higher T_c. At higher crystallization temperatures (~45 °C), the fully extended chain crystal has a melting temperature of ~66 °C. The melting temperatures reported above are at a heating rate of 20 °C/min. The melting temperatures corrected for heating rate are used to construct a Hoffman−Weeks plot of melting temperatures of crystals versus the crystallization temperature as shown in Figure 7. The equilibrium melting temperature is deduced from the extrapolation of T_m to a point where $T_m = T_c$. This corresponds to a state of zero driving force or equilibrium state of formation of the crystal. The equilibrium melting temperature of T^0_m = 63.2 °C agrees well with the value obtained for short chains by Kovacs.[4] Similarly, the equilibrium melting temperature of the high molecular weight fraction is 70.2 °C.

The peak area under the fully extended crystal melting (Figure 6c) is a strong function of the melting rate, increasing with decreasing rate. This suggests considerable recrystallization occurs during the ramping process. The effect is minimized at higher heating rates, as chains do not get time to recrystallize.

The phase behavior during crystallization of blends is seen from the melting endotherm of the 70/30 blend in Figure 6b. The melting endotherms of the 50/50 and 80/20 blends show features and trends similar to those of the 70/30 blend. At low temperatures of crystallization, all the blends have a single melting peak, corresponding to a single crystal population (corresponding also to a single crystallization peak). At higher T_c's, the DSC endotherm shows a double melting peak (corresponding to a broad crystallization exotherm with a shoulder). The effect of heating rate on the double melting peak has been studied. The two peaks are present at all heating rates from 5 to 30 °C/min. The total peak area remains the same for all heating rates, indicating that no new material crystallizes during the ramping process. The appearance of two crystal populations in the melting behavior of the blends suggests that the two components form two distinct phases and is not an artifact of the heating rate. The lower melting peak position does not change with the crystallization temperature, but the higher melting peak position does increase with increasing T_c. The enthalpy of fusion for the pure fractions and blends is shown in Figure 8. The smooth curves in the figure are the enthalpies of fusion

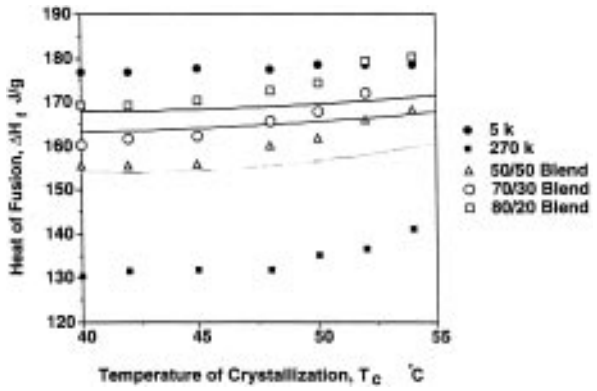

Figure 8. Heat of fusion determined from melting traces of pure fractions and blends. Lines are the weighted sum of pure fractions ΔH_f's. Symbols are the experimentally determined ΔH_f's for the blends.

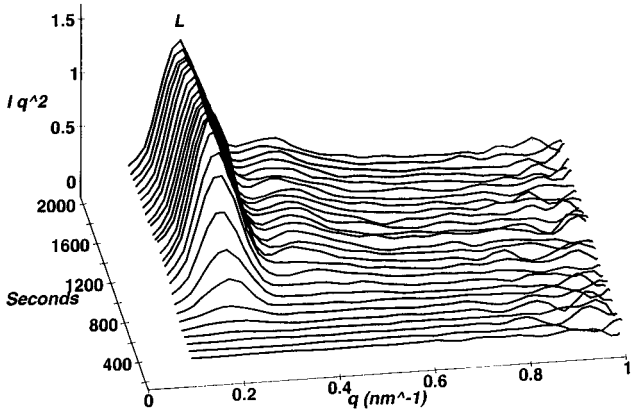

Figure 9. Lorentz-corrected SAXS data (Iq^2 *vs* q) for the 270K fraction at $T_c = 45$ °C. L denotes the long spacing of the 270K fraction.

calculated as the weighted sum of the pure fraction enthalpies. The symbols are the experimental enthalpies obtained from DSC endotherms. At all T_c's, both components crystallize. The heats of fusion for the blends are seen to increase at higher T_c toward the 5K value. A slower growth in blends at higher T_c's would result in more perfect crystals, leading to an increase in the enthalpy of fusion.

Time-resolved SAXS studies of isothermal crystallization of the pure fractions and blends were carried out to examine results obtained by DSC. The experiments were done for the same crystallization temperatures used for OM and DSC experiments.

Figure 9 shows a set of time-resolved scattering curves obtained during the crystallization of the high molecular weight fraction at $T_c = 45$ °C. The scattering peak corresponds to a long period of 31 nm (denoted as L in Figure 9). At higher T_c, a second-order peak develops. The peak position does not change with increasing time of crystallization. However, the peak position shifts to lower q values with increasing crystallization temperatures. The shift corresponds to an increase in crystal thickness with decreasing undercooling. At higher T_c, the driving force (ΔT) is lower, resulting in a lower number of folds of the polymer chain in the crystal lattice or a thicker crystal.

Figure 10 is a similar plot for the 5K polymer at 45 °C. The short-chain polymer can exist in any of the three configurations during crystallization: twice folded, once folded, and fully extended. The fully extended chain length is ~30 nm (IF = 0), the once-folded length

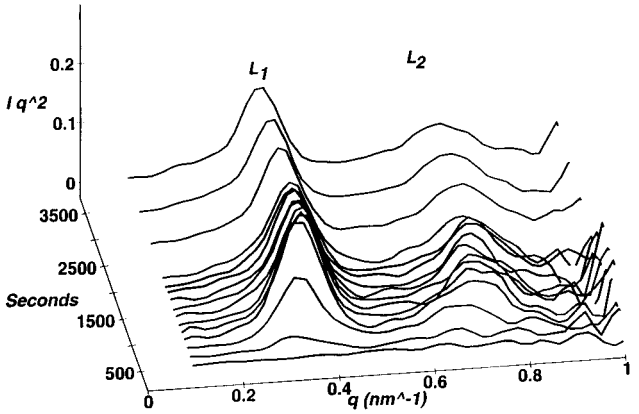

Figure 10. Lorentz-corrected SAXS data for the 5K fraction at $T_c = 42$ °C. L_1 is the final long spacing of the IF = 1 crystal, and L_2 is the final long spacing of the IF = 2 crystal.

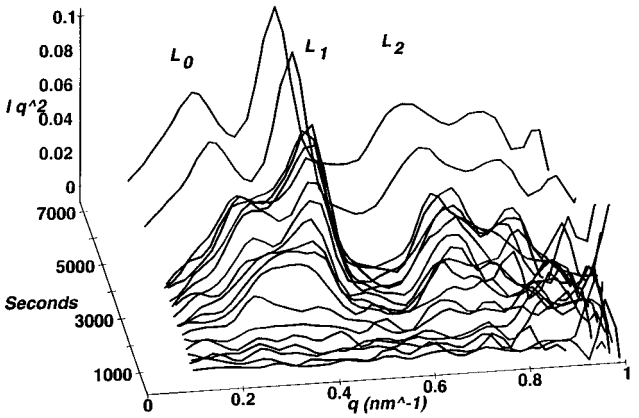

Figure 11. Lorentz-corrected SAXS data of the 5K fraction crystallizing at 50 °C. L_0 is the long spacing of the fully extended IF = 0 crystal. An intermediate-sized crystal NIF population at $q = 0.33$ nm^{-1} transforms to IF = 0 and IF = 1 crystal populations.

is ~15 nm, and the twice-folded length is ~10 nm (IF = 2). The crystallinities as deduced from DSC ($x_c = \Delta H_f/\Delta H_f^0 > 90\%$) are high, and the long period obtained from the scattering plot is identified with the crystal thickness. In the figures, the long periods associated with the IF = 0 crystal is marked as L_0, the IF = 1 crystal as L_1, and the IF = 2 crystal as L_2. At low T_c, the crystal thicknesses deduced from the scattering plot (Figure 10) are ~16 and ~9 nm and correspond to an IF = 1 crystal population and an IF = 2 population. Figure 11 shows SAXS during crystallization of the 5K chain at $T_c = 50$ °C. In this case, the early stages of crystallization exhibit one broad SAXS peak at ~18 nm. Later, this peak splits gradually into two peaks, corresponding to 20 and 12 nm. It is suggested that this splitting represents transformation from NIF to IF = 1 and IF = 0 crystals.

The results for the SAXS experiments on the pure fractions are summarized in Table 3. The long spacings for each fraction are tabulated as a function of the crystallization temperature. All values correspond to the final long spacing attained by the crystals, as recorded in the last file of the SAXS scan. The long spacing of the 270K fraction (L) increases gradually. The long spacing of the IF = 0, fully extended chain of the 5K fraction (L_0) appears only at higher temperatures of crystallization.

Figure 12 is a scattering plot for crystallization of the 70/30 blend at low T_c (42 °C). The scattering peaks

Table 3. Long Periods Obtained from Scattering Data of the Pure Fractions as a Function of the Crystallization Temperature[a]

long spacing (nm)	temp of crystallization (T_c (°C))					
	42	45	48	50	52	54
270K						
L	30.2	31.5	32.6	33.2	35.6	39.8
5K						
L_0			27	29.8		
L_1	16.8	16.8	15.8	15.7	15.7	
L_2	8.6	8.4	8.7	9.2	9.7	

[a] The long period of the 270K polymer is deonted as L. The long periods of 5K polymer are denoted as L_0 for the fully extended crystal (IF = 0), L_1 for the once-folded crystal (IF = 1), and L_2 for the twice-folded crystal (IF = 2).

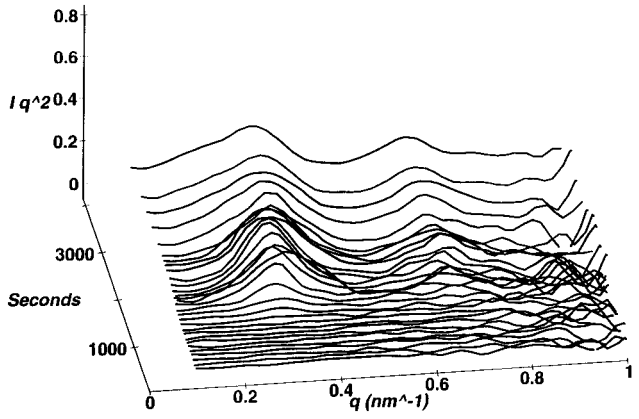

Figure 12. Time-resolved Lorentz-corrected SAXS plot of the 70/30 blend at $T_c = 42$ °C. An NIF cocrystal population forms at $q = 0.33$ nm^{-1} and thins to an IF = 1 cocrystal population.

corresponds to long spacings of 20 and 9 nm at the beginning. These likely represent NIF and IF = 2 crystal populations. The absence of a scattering peak at low angles suggests either that the high and low molecular weight components have cocrystallized into a NIF cocrystal or that only the low molecular weight component has crystallized. At higher T_c = 45 °C, Figure 13a, time-resolved scattering data for crystallization from this blend shows the dynamic phase separation of a NIF crystal population. The NIF cocrystal is formed at initial times with a long period of 17−19 nm. At later times, this crystal population transforms into two populations, with long periods ∼28 and ∼16 nm. The long period of ∼28 nm corresponds closely to that of the pure high fraction (∼31 nm) at the same T_c, and the long period of ∼16 nm corresponds to the IF = 1 crystal of the 5K fraction. The invariant (representing the volume transformed) for this experiment is shown in Figure 13b. The time of phase separation in the blend is marked. At higher T_c, two discrete crystal populations begin growing from the very start of crystallization, indicating the growth of two phases, as seen for $T_c = 50$ °C in Figure 14 for the 70/30 blend. In addition, there is a scattering peak corresponding to the IF = 2 crystal and a fourth peak, which we have interpreted as the second order of the second peak (L_2).

SAXS results for the 80/20 blend mimic those of the 70/30 system. At 45 °C, an NIF population splits into two new populations. At higher T_c's, this blend, like the 70/30 blend, shows these crystal populations from the start.

Results for the 50/50 blend show that two discrete crystal populations always exist at all $T_c > 42$ °C and the scattering plots are similar to Figure 14. At lower

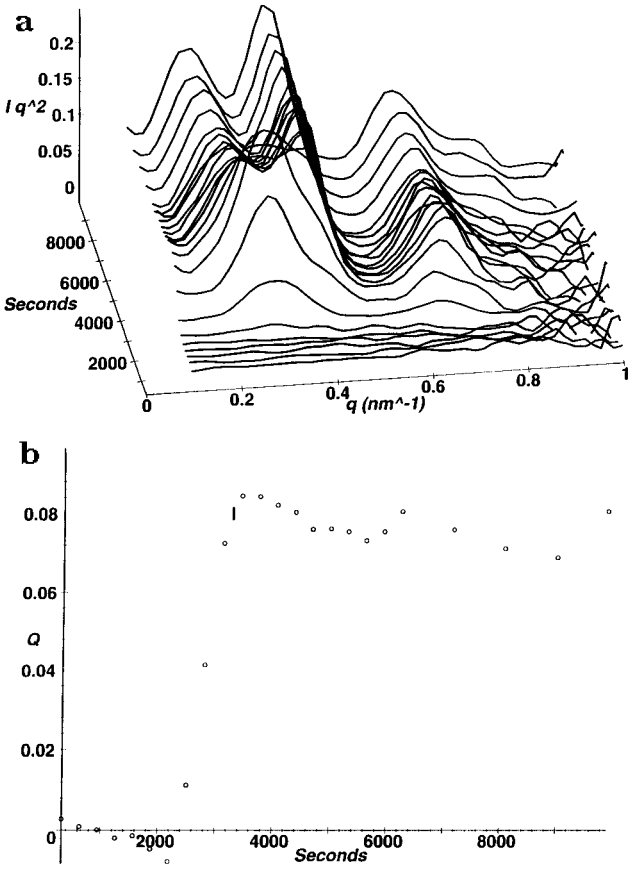

Figure 13. (a) Time-resolved, Lorentz-corrected SAXS plot of crystallization of the 70/30 blend at $T_c = 45$ °C. Dynamic phase separation of components from an NIF ($q = 0.33$ nm^{-1}) cocrystal to L and L_1, long spacings of the 270K crystal population and IF = 1 crystal population of the 5K polymer, respectively. (b) Integrated intensity of scattering (Q) vs time of crystallization for the 70/30 blend at $T_c = 45$ °C.

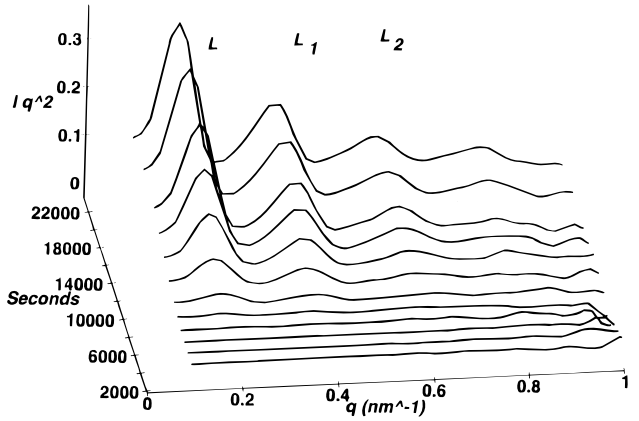

Figure 14. Lorentz-corrected SAXS plot of crystallization of 70/30 blend at $T_c = 50$ °C. The fourth peak ($q = 0.8$ nm^{-1}) is the second order of the L_1 peak.

T_c, Figure 15 shows that the 50/50 blend cocrystallizes to form a mixed crystal closer in thickness to the high molecular weight fraction.

4. Discussion

The crystallization behavior of the blends of high and low molecular weight PEO is strongly dependent on the crystallization temperature or alternatively on the degree of undercooling (ΔT). At high undercoolings, both components enter a common crystal lattice and at lower undercoolings, the components dynamically phase separate into two separate crystal phases. The mech-

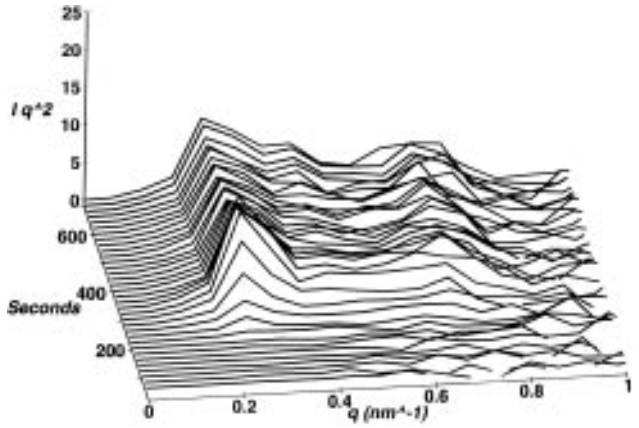

Figure 15. Lorentz-corrected SAXS plot of 50/50 blend at T_c = 40 °C. Cocrystal periodicity corresponds to a $q \sim 0.25$ nm^{-1}. Data were collected at the synchrotron light source (NSLS, Brookhaven).

anism of cocrystallization and phase separation is discussed in the context of results obtained by OM, DSC, and SAXS.

4.1. Cocrystallization. At low crystallization temperatures (~42 °C and below), the degree of undercooling for both components is well over 20 °C. The degree of undercooling is comparable and a large driving force exists for the growth of both components. The mutual diffusion of the components in the melt is relatively slow and the components do not have time to separate before crystallization occurs and a metastable solid solution is formed.

A good index for the formation of a solid solution is provided by the Peclet number for growth of the spherulite in the blend. The Peclet number is defined as $Pe = V/(D_m/R)$, where V is the spherulite growth velocity of the pure components, D_m is the mutual diffusivity in the blend, and R is the radius of the spherulite. D_m/R represents the diffusion velocity of the components. $V > D_m/R$, or $Pe > 1$, represents a condition in which the growth rate exceeds the diffusion rate. In this case, one expects cocrystallization. The growth velocities V of the pure components are comparable at 20−40 μm/s and the mutual diffusion coefficient, D_m (refer to the Appendix), is approximately 10^{-10} cm^2/s. The value of the Peclet number for growth is $\sim 10^3 R$ (R in μm) and is greater than 1 for even the smallest spherulite present.

The mechanism of cocrystallization can be speculated on from the results of OM, DSC, and SAXS. Optical microscopy results for the PEO pure fractions show that the low molecular weight component grows faster than the high molecular weight component. It would be expected that in this case crystallization in a blend should occur by the formation of templates of the low molecular weight crystal, followed by the addition of the high molecular weight component. The net result would be the formation of a cocrystal having the thickness of the pure low molecular weight crystal. The experimental evidence of a single crystallization peak (Figure 5), a single melting peak (Figure 6b) with T_m close to the pure low molecular weight fraction and a SAXS periodicity (Figure 12) corresponding to a thin crystal, confirm this picture. The cocrystals formed initially have a periodicity of ~20 nm, which corresponds to a defect structure, with chain ends of the low molecular weight fraction within the crystal. The crystals subsequently thin down, to have the chain ends completely excluded from the lattice (later time scans in Figure 12 indicate a decrease in periodicity). The other possibility is that only low molecular weight crystals form. This would also give rise to a single crystallization peak, a single melting peak, and a SAXS periodicity corresponding to a thin crystal. However, an easy method of distinguishing the two is provided by looking at the heat of fusion in a blend crystallized at these temperatures. In Figure 8, the heat of fusion at T_c = 42 °C is near the weighted sum of the heats of fusion of the two components, indicating that both components have crystallized to their normal extents.

The thickness of the cocrystal formed depends also on the blend composition. Blends containing a high percentage of low molecular weight fraction (70/30, 80/20) cocrystallize as thin crystals (Figure 12, $q \sim 0.3$ nm^{-1} and higher). At a blend composition of 50/50, the SAXS periodicity is closer to the high molecular weight chain crystal (Figure 15, $q \sim 0.25$ nm^{-1}). A possible explanation for this effect of composition relates to a competition between the energy of chain folding of long chains and the energy associated with inclusion of the ends of short chains within the crystal. At high volume fractions of the long chains, it may become energetically prohibitive to introduce the fold density necessary to form a thin crystal. Accommodation of chain end defects from the shorter chains would be less energy expensive. The net result would be a thicker cocrystal. As the volume fraction of short chains is increased, the introduction of a large number of chain end defects becomes energetically unfavorable compared to a low density of chain folding of long chains, the net result being the formation of thin crystals.

4.2. Phase Separation and Mechanism. At higher crystallization temperatures, the 70/30 and 80/20 blends show dynamic phase separation, as seen Figure 13a. An NIF crystal is first formed with a periodicity of ~20 nm. The crystal contains the long chain folded into the lattice of the shorter chain. The formation of the NIF cocrystal is controlled by energetics (as discussed in the previous paragraph) or the kinetics of attachment of both the components. The subsequent splitting of the SAXS periodicity into two periods is indicative of instability of the growth surface. The long spacing of the initially formed NIF cocrystal is completely replaced by two new long periods, one corresponding to the high molecular weight and the other to the IF = 1 crystal of the low molecular weight. As a first step in the mechanism of phase splitting, we propose that considerable sliding and rearrangement of the long and short chains takes place in the NIF cocrystal, destroying the original periodicity. Factors leading to such rearrangement include the following: (1) The NIF cocrystal would require a high density of the ends of short chains within the crystal. Included chain ends are defects which raise the free energy of formation of the NIF crystal. To minimize the free energy of the crystal, short chains have to have their chain ends completely excluded from the lattice. The formation of the IF = 1 periodicity in the SAXS peak (Figure 13a) corresponding to the pure low molecular weight crystal confirms that such a driving force does exist. (2) The fold length of the high molecular weight chain is small in the cocrystal and the number of folds is large. Once again, since most of the undercooling goes to folding chains, a large number of folds would mean a higher free energy of formation of the NIF cocrystal. The system tries to minimize its energy by rearrangement into thicker crystals of the high molecular weight chains. The stable stem length of the pure high molecular weight chain at a given T_c corresponds

to a periodicity of ~28 nm or larger. The long chains in the NIF cocrystal will tend to thicken to a similar value if annealed isothermally. (3) The rearrangement should also be dependent on the size of the short chains. The thinning of short chains involves sliding short chains out from among the long chains in the NIF cocrystal. A short length would facilitate easier phase separation than if the chains were longer.

Rearrangement of chains is not a sufficient explanation for the appearance of two SAXS periodicities for the blend. We denote the high molecular weight crystal as 1 and the low molecular weight IF = 1 crystal as 2. It is clear that whenever we have strong 11 and 22 correlations, the resulting SAXS pattern would contain the corresponding periodicities. This would correspond to a case of separate phase areas of the two components within a spherulite of the blend. If, however, the two crystals are mixed together randomly or there is an interleaving of crystals, scattering would lead to a major peak corresponding to the average repeat distance[27−29] (this peak would overlay the second-order scattering from the initial population). In addition, we can expect a weak scattering correlation between the thinner crystals that are distributed randomly to show up as a small peak or a hump in the scattering curve at low angles of scattering. During the crystallization of the blend, if the entire volume of the sample crystallizes as an NIF cocrystal and subsequently transforms to two crystal populations, randomly interleaved, the corresponding scattering pattern in the later time scans would result in a single periodicity. However, the results of phase separation seen in Figure 13a is the development of two discrete long periods corresponding to the pure fraction long periods. Also, there does not exist a low-angle peak or hump that would be associated with scattering from thin crystals in a randomly interleaved population. Recall also that the separation of the lamellar system into two long-period populations occurs before spherulites have filled the volume as evidenced in the small-angle invariant results (Figure 13b). Transformed crystals at the solid/melt interface would provide templates for the further addition of the two components. The templates of each of the phases would provide separate coherent nucleation sites of the "correct" substrate length for the high and low molecular weight chains. Segregation of the components by diffusion and crystallization on the template crystals would then spawn new crystals of the same type, resulting in stacks of crystals of the same type and in two periodicities.

The mechanism of phase separation is summarized in Figure 16. Figure 16a depicts the formation of the NIF cocrystal containing both the components. The shorter chains have their chain ends included within the crystal and the longer chains would have considerable slack associated with nonfolded parts of the chain. Figure 16b depicts a thinning and thickening of short and long chains, respectively. Figure 16c depicts the formation of a template of each crystal of short and long chains, and Figure 16d shows the spawning of separate crystal stacks of each component due to segregation of the components followed by crystallization on templates. The SAXS evidence for the proposed mechanism of phase splitting is complemented by DSC. The blend crystallizes with a broad single exotherm, corresponding to the formation of the NIF cocrystals (Figure 5). The melting endotherm of annealed crystals shows a double melting peak (Figure 6b). The double melting peak

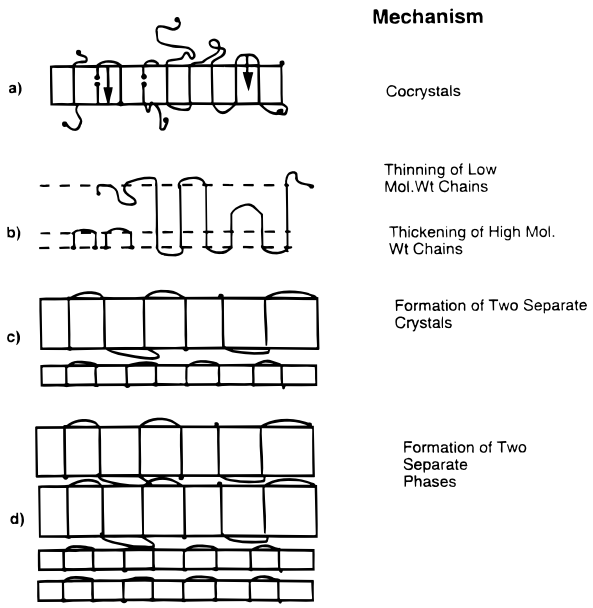

Figure 16. Mechanism of phase segregation: (a) formation of NIF cocrystal of both components; (b) thickening of long chains of the high molecular weight and thinning of short chains; (c) templates of high and low molecular weight crystals are formed onto which new chains add; (d) spawning of separate crystals of high and low molecular weight polymer. The process is aided by diffusion of components to separate crystal sites.

corresponds to the thick and thin crystals of each of the components, complementing the two periodicities seen in the SAXS experiment (Figure 13a).

At higher crystallization temperatures, or lower degrees of undercooling, the components crystallize cooperatively into separate phase areas. At these higher temperatures, diffusion rates are enhanced and phase segregation can be achieved easily. The crystallization rates of the pure fractions differ considerably, and one would expect sequential rather than simultaneous growth of the two components during crystallization of blends. It is however seen from results of OM (Figure 3b) and DSC crystallization exotherms (Figure 5 at T_c = 48 °C) that both components crystallize simultaneously. A possible reason for this behavior is that the faster growing component (the high molecular weight polymer) provides nucleation sites for the addition of low molecular weight chains. Again, only a few templates are needed for the formation of a coherent phase of the low molecular weight component. Phase separation is also energetically favorable at lower undercoolings as compared to the penalty of high free energy of formation of cocrystals and their subsequent phase separation. The heats of fusion for the blends indicates that both components crystallize completely (Figure 8). The growth of adjacent phases would also mean that a diffusion couple is established for the two components, resulting in component segregation followed by crystallization into separate phases. Growth of this nature can be termed "eutectic-like".

The phase behavior of crystallization can be summarized by the plot of melting temperatures of the 70/30 blend as a function of the crystallization temperature in Figure 17a. Phase splitting results in two melting peaks. The corresponding SAXS long spacings are summarized in Figure 17b. Results for the 80/20 blend are similar to those for the 70/30 blend. For the 80/20 blend, however, the temperature at which phase separation occurs is higher (~45 °C) and the melting point

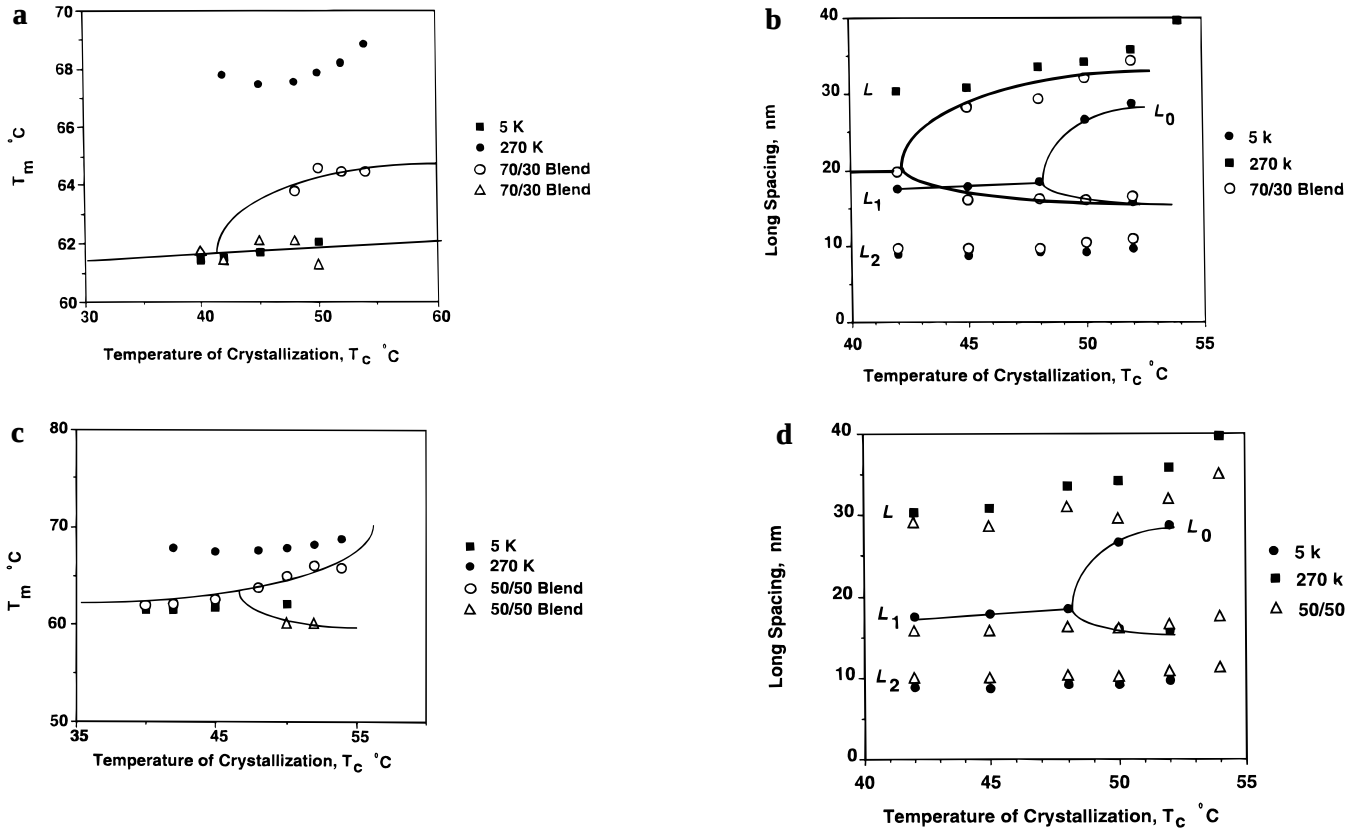

Figure 17. (a, c) Melting temperatures of blends, crystallized at increasing T_c. Phase splitting is indicated by the fork in the diagram. (b, d) Long spacings of different crystal populations (denoted as L, L_0, L_1, and L_2) obtained by SAXS of the blends with increasing T_c. The inner fork corresponds to NIF crystal transformation of the 5K chain to a once-folded and a fully extended chain.

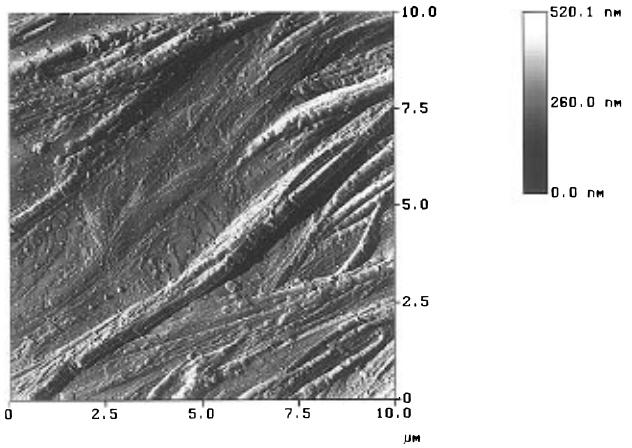

Figure 18. Morphology of crystallization in a 80/20 blend at $T_c = 48$ °C. Atomic force microscopy of a preferentially etched sample reveals high molecular weight crystal bundles separated by a low molecular weight crystal phase.

of the lower melting phase is indistinguishable from that of the neat 5K polymer. The phase behavior of the 50/50 blend is similar to the above; phase separation manifests at all temperatures studied (Figure 17c,d). Morphological evidence for this model is obtained from atomic force microscopy (AFM). Figure 18 is an AFM image of an etched surface of a 80/20 blend crystallized at 48 °C. Preferential etching of the crystallized components shows two distinct areas, one of which is compact bundles which stand out on etching and the other a highly etched region. The compact bundles are taken to be the high molecular weight polymer and the highly etched region the low molecular weight polymer. This is substantially the alternating bundle microstructure postulated in Figure 16d.

5. Conclusions

The study of blends of high and low molecular weight PEO by DSC, OM, and time-resolved SAXS indicates that both components cocrystallize at high undercoolings. The mechanism of cocrystallization is due to the low molecular weight chains providing templates onto which the high molecular weight chains fold. This is true of blends with a high volume fraction of low molecular weight chains. As the weight fraction of long chains is increased, the cocrystals become thicker. At higher crystallization temperatures, both components cocrystallize to form an NIF cocrystal. The long-chain molecules in the cocrystal gradually separate, to form thicker crystals, while the short-chain molecules simultaneously separate to form thinner crystals, resulting eventually in the formation of separate phases (separate lamellar stacks). Further, increasing the temperature of crystallization results in cooperative growth of separate phases within a spherulite. The cooperative growth is eutectic-like in nature.

Acknowledgment. We gratefully acknowledge financial support by NSF under Grant DMR-9115308.

Appendix

The mutual diffusion of chemically identical polymers of short chains (A) diffusing into long chains (B) is given as[30]

$$D_m = (1 - \phi)D_A + \phi D_B \qquad (2)$$

where $D_A = (N_A^2/N_e)D_A^*[(1 - \phi)/N_A + \phi/N_B]$ and $D_B = N_B/(1 - \phi)D_B^*[(1 - \phi)/N_A + \phi/N_B]$ are the intrinsic diffusion coefficients of A and B species. N_A and N_B are the number of monomer units in A and B polymer. N_e is the number of monomer units for a polymer which is just entangled. D_A^* and D_B^* are the self-diffusion coefficients of the two species. ϕ is the volume fraction of the low molecular weight species denoted by A. The critical entanglement molecular weight for PEO is $M_e = 4400$.[31] This corresponds to an N_e value of 100. The number of monomers in the short chain (5K) is $N_A = 114$ and for the long chain (270K) is $N_B = 6136$. The self-diffusivity of the small chain is calculated as $D_A^* = 6.65 \times 10^{-5} \exp[-23000/(RT)]$ cm^2/s[32] and the self-diffusivity of the 270K fraction as $D_B^* = 1.03 \times 10^{-9} \exp[-16000/(RT)]$ cm^2/s.[31] The value of the activation energy of 16 kJ/mol is extrapolated from Figure 5 of ref 31.

The mutual diffusion coefficients for the blends of 5K and 270K as calculated from the above equation are $\sim 10^{-10}$ cm^2/s at 42 °C and $\sim 10^{-9}$ cm^2/s at 52 °C.

References and Notes

(1) Kovacs, A. J.; Gonthier, A. *Kolloid Z. Z. Polym.* **1972**, *250*, 530.
(2) Kovacs, A. J.; Gonthier, A.; Straupe, C. *J. Polym. Sci., Polym. Symp.* **1975**, *50*, 283.
(3) Kovacs, A. J.; Straupe, C.; Gonthier, A. J. *J. Polym. Sci., Polym. Symp.* **1977**, *59*, 31.
(4) Kovacs, A. J.; Buckley, C. P. *Colloid Polym. Sci.* **1976**, *254*, 695.
(5) Cheng, S. Z. D.; Zhang, A.; Chen, J. *J. Polym. Sci., Polym. Lett. Ed.* **1990**, *28*, 233.
(6) Cheng, S. Z. D.; Zhang, A.; Chen, J.; Herberer, D. P. *J. Polym. Sci., Polym. Phys. Ed.* **1991**, *29*, 287.
(7) Cheng, S. Z. D.; Zhang, A.; Barley, J. S.; Chen, J.; Habenschuss, A.; Zschack, P. R. *Macromolecules* **1991**, *24*, 3937.
(8) Ashman, P. C.; Booth, C. *Polymer* **1973**, *14*, 300.
(9) Hartley, A.; Leung, Y. K.; Booth, C.; Shepherd, I. W. *Polymer* **1976**, *17*, 354.
(10) Fraser, M. J.; Marshall, A.; Booth, C. *Polymer* **1977**, *18*, 93.
(11) Cheng, S. Z. D.; Chen, J.; Zhang, A.; Herberer, D. P. *J. Polym. Sci., Polym. Phys. Ed.* **1991**, *29*, 299.
(12) Cheng, S. Z. D.; Scott, S. W.; Chen, J.; Zhuo, Q.; Quirk, R. P.; von Meerwall, E. D.; Hsiao, B.; Habenschuss, A.; Zschack, P. R. *Macromolecules* **1993**, *26*, 5105.
(13) Allen, R. C.; Mandelkern, L. *J. Polym. Sci., Polym. Phys. Ed.* **1982**, *20*, 1465.
(14) Mandelkern, L.; Stack, G. M. *Macromolecules* **1984**, *17*, 871.
(15) Hoffman, J. D.; Frolen, L. J.; Ross, G. S.; Lauritzen, J. I., Jr. *J. Res. Natl. Bur. Stand.* **1975**, *79A*, 671.
(16) Hoffman, J. D. *Polymer* **1982**, *23*, 656.
(17) Cheng, S. Z. D.; Chen, J.; Janimak, J. J. *Polymer* **1990**, *31*, 1018.
(18) Hoffman, J. D. *Polymer* **1983**, *24*, 3.
(19) Cheng, S. Z. D.; Wunderlich, B. *J. Polym. Sci., Polym. Phys. Ed.* **1986**, *24*, 577.
(20) Cheng, S. Z. D.; Wunderlich, B. *J. Polym. Sci., Polym. Phys. Ed.* **1986**, *24*, 595.
(21) Cheng, S. Z. D.; Bu, H. S.; Wunderlich, B. *J. Polym. Sci., Polym. Phys. Ed.* **1988**, *26*, 1947.
(22) Bu, H. S.; Cheng, S. Z. D.; Wunderlich, B. *Polym. Bull.* **1987**, *16*, 567.
(23) Bu, H. S.; Cheng, S. Z. D.; Wunderlich, B. *Polymer* **1988**, *29*, 579.
(24) Wignall, G. D.; Lin, J. S.; Spooner, S. *J. Appl. Crystallogr.* **1990**, *23*, 241.
(25) Hendricks, R. W. *J. Appl. Crystallogr.* **1978**, *11*, 15.
(26) Song, H. H.; Stein, R. S.; Ree, M.; Phillips, J. C.; Le Grand, A.; Chu, B. *Macromolecules* **1988**, *21*, 1180.
(27) Stein, R. S. *Pure Appl. Chem.* **1991**, *63*, 941.
(28) Tashiro, K.; Satkowski, M. M.; Stein, R. S.; Lie, Y.; Chu, B.; Hsu, S. L. *Macromolecules* **1992**, *25*, 1801.
(29) Wignall, G. D.; Londono, J. D.; Lin, J. S.; Alamo, R. G.; Galante, M. J.; Mandelkern, L. *Macromolecules* **1995**, *28*, 3156.
(30) Kramer, E. J.; Green, P.; Palmstrom, C. J. *Polymer* **1984**, *25*, 473.
(31) Te Huirua, W. M.; Wang, R.; Callaghan, P. T. *Macromolecules* **1990**, *23*, 1658.
(32) Cheng, S. Z. D.; Barley, J. S.; von Meerwall, E. *J. Polym. Sci., Polym. Phys. Ed.* **1991**, *29*, 515.

MA960678S